Tetrahedron: *Asymmetry* 20 (2009) 733–740

Contents lists available at ScienceDirect

Tetrahedron: *Asymmetry*

journal homepage: www.elsevier.com/locate/tetasy

Amide-1,2,3-triazole bioisosterism: the glycogen phosphorylase case

Evangelia D. Chrysina [a,*], Éva Bokor [b], Kyra-Melinda Alexacou [a], Maria-Despoina Charavgi [a], George N. Oikonomakos [a], Spyros E. Zographos [a], Demetres D. Leonidas [a], Nikos G. Oikonomakos [a,†], László Somsák [b,*]

[a] *Institute of Organic and Pharmaceutical Chemistry, The National Hellenic Research Foundation, 48 Vassileos Constantinou Avenue, GR-116 35 Athens, Greece*
[b] *Department of Organic Chemistry, University of Debrecen, Egyetem tér 1, H-4032 Debrecen, Hungary*

ARTICLE INFO

Article history:
Received 4 February 2009
Accepted 19 March 2009
Available online 22 April 2009

Dedicated to George W. J. Fleet on the occasion of his 65th birthday

ABSTRACT

Per-O-acetylated β-D-glucopyranosyl azide was transformed into an intermediate iminophosphorane by PMe_3 which was then acylated to *N*-acyl-β-D-glucopyranosylamines. The same azide and substituted acetylenes gave 1-(β-D-glucopyranosyl)-4-substituted-1,2,3-triazoles in Cu(I)-catalyzed azide–alkyne cycloadditions. Deprotection of these products by the Zemplén method furnished β-D-Glc_p-NHCO-R derivatives as well as 1-(β-D-Glc_p)-4-R-1,2,3-triazoles which were evaluated as inhibitors of rabbit muscle glycogen phosphorylase b. Pairs of amides versus triazoles with the same R group displayed similar inhibition constants. X-ray crystallographic studies on the enzyme–inhibitor complexes revealed high similarities in the binding of pairs with R = 2-naphthyl and hydroxymethyl, while for the R = Ph and 1-naphthyl compounds a different orientation of the aromatic part and changes in the conformation of the 280s loop were observed. By this study new examples of amide-1,2,3-triazole bioisosteric relationship have been provided.

1. Introduction

Bioisosterism is a widely accepted principle in medicinal chemistry used to make changes in a lead structure with the aim of achieving various goals such as improved chemical stability or better pharmacokinetic properties while maintaining or even enhancing biological activity.[1–3]

In relation to the recent widespread use of the copper(I)-catalyzed azide-acetylene cycloaddition reaction[4,5] for the selective creation of 1,4-disubstituted 1,2,3-triazole derivatives, more and more examples show the similarity of the amide moiety and the 1,2,3-triazole ring.[6–8] The similitudes of the two moieties can be seen in the size (distance between substituents 3.8–3.9 Å in amides, 5.0–5.1 Å in triazoles), the dipolar character (amide ~4 Debye, triazole ~5 Debye) and the H-bond acceptor capacity (lone pairs of the amide O as well as of the triazole nitrogens as illustrated in **A** and **B**).[4] The triazole C(5)–H was suggested to act as a H-bond donor similar to the amide NH,[7] and it was shown by X-ray crystallography that the 1,2,3-triazole can participate in the H-bond network of an α-helical peptide.[6]

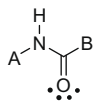

A

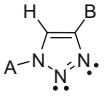

B

These findings raise the possibility of a broader use of the 1,2,3-triazole moiety as a bioisosteric replacement[1–3] for the amide group. This is also supported by the high chemical stability of the 1,2,3-triazole ring especially under hydrolytic as well as reductive and oxidative conditions. However, the outcome of such a replacement may depend on the biological target, that is, this kind of isosterism may not be considered to be obvious and it should be verified in each case. In this paper we investigate the amide → 1,2,3-triazole modification in inhibitors of rabbit muscle unphosphorylated glycogen phosphorylase (RMGP*b*) enzyme, a molecular target for the control of hyperglycaemia in type 2 diabetes (80% homologous with the liver isoform).[9–12]

2. Results and discussion

A large series of *N*-acyl-β-D-glucopyranosylamines **5** were prepared and investigated as inhibitors of RMGP*b*[11–14] which lend themselves to bioisosteric modification as in **3**. For both series of compounds the O-peracetylated glucopyranosyl azide **1** can be used as the starting material (Table 1). Thus, **1** was transformed via Cu(I)-catalyzed azide-acetylene cycloadditions into 1-(2,3,4,6-

* Corresponding authors. Tel.: +30 210 727 3851; fax: +30 2107273831 (E.D.C.); tel.: +36 52 512 900x22348; fax: +36 52 453 836 (L.S.).
E-mail addresses: echrysina@eie.gr (E.D. Chrysina), somsak@tigris.unideb.hu (L. Somsák).
† Deceased on August 31, 2008.

0957-4166/$ - see front matter © 2009 Elsevier Ltd. All rights reserved.
doi:10.1016/j.tetasy.2009.03.021

Table 1
Synthesis and crystallographic numbering of 1-(β-D-glucopyranosyl)-4-substituted-1,2,3-triazoles **3** and *N*-acyl-β-D-glucopyranosylamines **5** and their inhibitory effect (K_i) against rabbit muscle GP*b* (RMGP*b*)

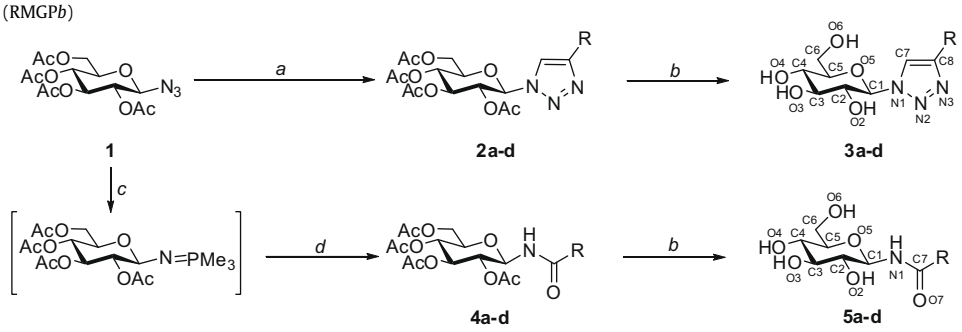

a) R-C≡CH, $CuSO_4$, ascorbic acid, water, 70 °C, 8 h; *b*) NaOMe (cat.), MeOH, r.t.; *c*) PMe_3, dry CH_2Cl_2, r.t., ~10 min., followed by *d*) RCOOH in CH_2Cl_2, r.t.

	R	**2** (%)	**3** (%)	K_i (μM)	**4** (%)	**5** (%)	K_i (μM)
a	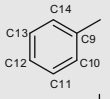	58[a]	89[b,17]	151.3 ± 2.3	91[15]	98[16]	81[13] 144[16]
b	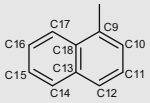	66	95[18]	135.9 ± 9.5	52[14]	75[14]	190.7 ± 23.7 444[14]
c	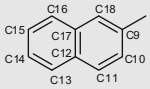	71	72[19]	16.1 ± 1.3	62[14]	92[14]	12.8 ± 1.6 10[14]
d	$-CH_2OAc$ in **4** $-CH_2OH$ in **2,3 and 5**	65[c]	82[c,20]	13.7 ± 1	64[21]	86[22]	17.9 ± 0.4

[a] For other preparations see Refs. 23–25.
[b] For other preparation see Ref. 25.
[c] For other preparation see Ref. 26.

tetra-*O*-acetyl-β-D-glucopyranosyl)-4-substituted-1,2,3-triazoles **2a**–**d** which were deprotected by using the Zemplén protocol to give the test compounds **3a**–**d**. The series of amides **5a**–**d** was obtained by acylation of an iminophosphorane prepared from **1** by PMe_3 and subsequent removal of the acetyl protecting groups from **4a**–**d** by the Zemplén method as described earlier.[14–16]

Compounds **3a**–**d** and **5a**–**d** were assayed in the direction of glycogen synthesis for their inhibitory effect on RMGP*b* (Table 1) as described previously.[27,28] Each compound exhibited competitive inhibition with respect to the substrate glucose-1-phosphate, at constant concentrations of glycogen (0.2% w/v) and AMP (1 mM). Comparison of the inhibition constants (K_i) measured for triazoles **3** to those of amides **5** having the same R groups showed reasonable agreement for the two series.

Structural studies of both sets of compounds were performed to delineate their inhibitory potency for RMGP*b*. Crystallographic data collection, processing and refinement statistics for the structure determination of each compound are summarized in Table 2.

RMGP*b* is an allosteric enzyme with distinct binding sites that are exploited for the design of new hypoglycaemic agents employing the structure-based inhibitor design approach. In particular, the catalytic site of RMGP*b* is a long channel filled with water molecules in the native enzyme, the entrance of which is blocked by a flexible loop, 280s comprising residues 282–287. It is dissected into two subsites one lying next to the 280s loop (β-pocket) and a smaller subsite for β-C-1 and α-C-1 substituents, respectively.[32] All triazole and amide ligands are bound at the catalytic site of RMGP*b* as suggested by both the $2F_o - F_c$ and $F_o - F_c$ difference electron density maps, forming the characteristic hydrogen bond interactions between the peripheral hydroxyl groups of glucopyranose and the residues lining the site. In the case of amide ligands the hydrogen bond interaction[34,35] between the amide group attached to the C1 position of the pyranose ring and the backbone O of His377 characteristic for many glucose analogues is also maintained in this series (compounds **5a**–**5d**). Schematic diagrams of the network of hydrogen bond interactions formed at the catalytic site of the enzyme upon binding of compounds **3a**–**d** and **5a**, **5d** are shown in Figure 1. Structural similarities and differences in the enzyme-inhibitor complexes are illustrated by superpositions of the relevant pairs shown in Figure 2.

2.1. Crystallographic studies: 3c versus 5c

More specifically, **3a** binds at the catalytic site of the enzyme forming 13 hydrogen bonds and 83 van der Waals interactions (Fig. 1a). A DMSO molecule was also bound at the same site as suggested by the electron density difference maps. It is mainly involved in van der Waals interactions with O2 of the glucopyranose ring and the three nitrogens of the triazole moiety. A number of changes are induced upon binding of **3a** to the catalytic site, especially in residues coming from the 280s loop, compared to the corresponding amide analogue. The three dimensional structure of the latter was first determined in 1995 (at 2.3 Å resolution)[13] using X-ray data collected in house. A slightly improved version of that amide crystal structure (RMGP*b*-**5a**, data collected at 2.1 Å resolution using SRS) is presented here. The changes observed between the crystal structures of RMGP*b*-**3a** and RMGP*b*-**5a** are summarized as follows: all glucopyranose atoms lie almost at identical positions at the cata-

Table 2
X-ray crystallographic analysis[a] of 1-(β-D-glucopyranosyl)-4-substituted-1,2,3-triazoles **3a–d** and *N*-acyl-β-D-glucopyranosylamines **5a,d** in complex with T-state RMGP*b*

	3a	**3b**	**3c**	**3d**	**5a**	**5d**
Data collection and processing statistics						
Experiment	T-state RMGP*b* soaked with 20 mM of **3a** in 20% DMSO for 5 h	T-state RMGP*b* soaked with 10 mM of **3b** in 10% DMSO for 5 h	T-state RMGP*b* soaked with 10 mM of **3c** in 10% DMSO for 5 h	T-state RMGP*b* soaked with 100 mM of **3d** for 2 h	T-state RMGP*b* soaked with 100 mM of **5a** for 5 h	T-state RMGP*b* soaked with 20 mM of **5d** in 20% DMSO for 4 h and 45 min
No of images (°)	89 (89°)	80 (64°)	65 (52°)	100 (100°)	86 (68.8°)	89 (89°)
Spacegroup	$P4_32_12$	$P4_32_12$	$P4_32_12$	$P4_32_12$	$P4_32_12$	$P4_32_12$
Unit cell dimensions	$a = b = 127.3$ Å, $c = 115.6$ Å, $\alpha = \beta = \gamma = 90°$	$a = b = 128.8$ Å, $c = 116.2$ Å, $\alpha = \beta = \gamma = 90°$	$a = b = 128.8$ Å, $c = 116.7$ Å, $\alpha = \beta = \gamma = 90°$	$a = b = 127.2$ Å, $c = 115.1$ Å, $\alpha = \beta = \gamma = 90°$	$a = b = 128.6$ Å, $c = 116.3$ Å, $\alpha = \beta = \gamma = 90°$	$a = b = 127.2$ Å, $c = 115.3$ Å, $\alpha = \beta = \gamma = 90°$
Resolution (Å)	30.0–2.03	30.0–2.3	30.0–2.0	30.0–1.97	30.0–2.10	30.0–2.15
No of observations	796,448	538,382	702,140	994,252	920,874	660,645
No of unique reflections	60,007 (2991)	43,536 (2120)	65,215 (3044)	62,955 (3049)	56,904 (2851)	49,394 (2209)
R_m (outermost shell)[b]	0.063 (0.551)	0.091 (0.501)	0.069 (0.458)	0.062 (0.476)	0.059 (0.478)	0.088 (0.552)
Completeness (outermost shell) (%)	96.7 (98.3)	99.0 (98.6)	97.9 (93.4)	98.0 (96.5)	99.0 (100)	94.4 (86.4)
Outermost shell (Å)	2.06–2.03	2.34–2.30	2.03–2.0	2.03–2.0	2.14–2.10	2.19–2.15
$\langle I/\sigma(I)\rangle$ (outermost shell)[c]	11.5 (4.3)	19. 9 (3.9)	11.3 (3.3)	14.5 (4.2)	14.2 (5.1)	6.1 (2.3)
Redundancy (outermost shell)	5.9 (5.8)	5.3 (5.3)	4.1 (3.3)	5.5 (4.2)	5.6 (5.6)	3.5 (2.5)
B-values (Å^2) (Wilson plot)	32.5	30.8	32.7	26.5	31.6	36.0
Refinement statistics and model quality						
Resolution range (Å)	29.83–2.03	90.91–2.30	90.91–2.0	25.98–2.0	90.91–2.10	29.8–2.14
No of reflections used (free)	56,675 (3049)	41,320 (2193)	61,866 (3315)	59,682 (3190)	53,971 (2886)	46,809 (2523)
Residues included	(12–251) (261–314) (324–836)	(12–254) (261–314) (324–836)	(12–254) (261–314) (324–836)	(12–254) (261–314) (324–836)	(12–254) (258–317) (324–836)	(12–254) (261–314) (324–836)
No of protein atoms	6562	6589	6589	6597	6638	6604
No of water molecules	216	294	205	282	228	217
No of heteroatoms	22 (**3a**), 15 (PLP), 23 (IMP), 4 DMSO	26 (**3b**), 15 (PLP)	26 (**3c**), 15 (PLP)	18 (**3d**), 15 (PLP)	20 (**5a**), 15 (PLP)	16 (**5b**), 15 (PLP)
Final R (R_{free})[d]	0.196 (0.220)	0.174 (0.211)	0.197 (0.224)	0.195 (0.225)	0.197 (0.227)	0.193 (0.225)
R (R_{free}) (outermost shell)	0.252 (0.290)	0.218 (0.285)	0.261 (0.293)	0.255 (0.286)	0.243 (0.305)	0.253 (0.332)
r.m.s.d. in bond lengths (Å)	0.006	0.008	0.007	0.006	0.008	0.007
r.m.s.d. in bond angles (°)	1.035	1.085	1.032	1.015	1.044	1.054
Average B (Å^2) for residues	(12–251) (261–314) (324–836)	(12–254) (261–314) (324–836)	(12–254) (261–314) (324–836)	(12–254) (261–314) (324–836)	(12–254) (258–317) (324–836)	(12–254) (261–314) (324–836)
Overall	37.0	27.9	38.9	31.1	36.7	38.5
Ca, C, N, O	36.2	27.1	38.0	30.3	35.9	39.2
Side chain	37.9	28.6	39.7	31.9	37.5	38.5
Average B (Å^2) for heteroatoms	28.4 (**3a**), 29.1 (PLP) 48.0 (DMSO) 80.6 (IMP)	24.1 (**3b**), 16.5 (PLP)	34.5 (**3c**), 28.1 (PLP)	21.9 (**3d**), 20.4 (PLP)	29.1 (**5a**), 25.6 (PLP)	30.5 (**5d**), 28.3 (PLP)
Average B (Å^2) for water molecules	39.7	31.4	39.8	36.2	38.1	40.3

[a] Native T-state RMGP*b* crystals, grown in the tetragonal lattice, spacegroup $P4_32_12$[29] were soaked with various concentrations of inhibitors in buffered solutions at pH 6.7 in the presence of DMSO depending on their solubility. X-ray diffraction data were collected using synchrotron radiation sources at Daresbury Laboratory, UK and EMBL-Hamburg outstation and processed with the HKL package.[30] Complex structure determination and analysis were performed according to standard protocols as implemented in the CCP4 package.[31] The coordinates have been deposited with Protein Data Bank with pdb codes: **3a** = 3G2H, **3b** = 3G2L, **3c** = 3G2 K, **3d** = 3G2I, **5a** = 3G2N, **5d** = 3G2J. Detailed structural analyses for complexes of RMGP*b* with **5b** and **5c** will be published elsewhere.

[b] $R_m = \sum_i\sum_h|\langle I_h\rangle - I_{ih}|/\sum_i\sum_h I_h$, where $\langle I_h\rangle$ and I_{ih} are the mean and the *i*th measurement of intensity for reflection *h*, respectively.

[c] $\sigma(I)$ is the standard deviation of *I*.

[d] Crystallographic $R = \sum||\mathbf{F}_o| - |\mathbf{F}_c||/\sum|F_o|$, where $|F_o|$ and $|F_c|$ are the observed and calculated structure factor amplitudes, respectively. R_{free} is the corresponding (R) value for a randomly chosen 5% of the reflections that were not included in the refinement.

lytic site of the enzyme except C1 that shifts by ~0.6 Å to best accommodate the triazole ring and maintain the orientation of the rest of the ligand atoms along the catalytic channel. The nitrogen atoms N2 and N3 of **3a** form water-meditated interactions with residues from the glycine-rich helix (residues 130–137) Gly134 N and Gly137 N and Glu88 OE2 (through waters Wat204 O and Wat87 O). Focusing on **3a** phenyl group, it is subjected to a rotation of ~25° and the corresponding atom shifts vary from ~0.7 to ~1.0 Å resulting in displacement of a water molecule (Wat200 O in RMGP*b*-**5a** structure). This adjustment of the aromatic ring is due to both binding of a DMSO molecule, that has been identified and included in the structure next to this group and interrelated modifications observed in the residues of the 280s loop. A DMSO molecule is actually located in the position previously occupied by the Asn284 side chain in the RMGP*b*-**5a** complex structure. The new orientation adopted by the Asn284 side chain is mainly responsible for the rearrangement of the rest of the 280s loop residues to comply with stereochemical conditions. In more detail, these changes involve Asn282 (Cα atom shifts by ~1.0 Å and torsion angle (χ1) rotates by 122°), Asp283 (Cα moves by ~1.4 Å and torsion angles (ψ, χ1, χ2) rotate by (~104, 138, 99) degrees), Asn284 (Cα moves by ~2.8 Å and torsion angles (φ, ψ, χ1, χ2) rotate by (~167, 99, 121, 32) degrees) the side chain of which is now sandwiched between Phe285 and Tyr613 at the catalytic site of RMGP*b*. This results in changes in Phe285 (Cα shifts by ~1.8 Å and torsions (φ, ψ) rotate by (~32, 30°) to make sufficient space for Asn284 side chain and Phe286 (only N shifts by ~0.5 Å). Although the ligand atoms form no direct hydrogen bond interactions with the residues lining the

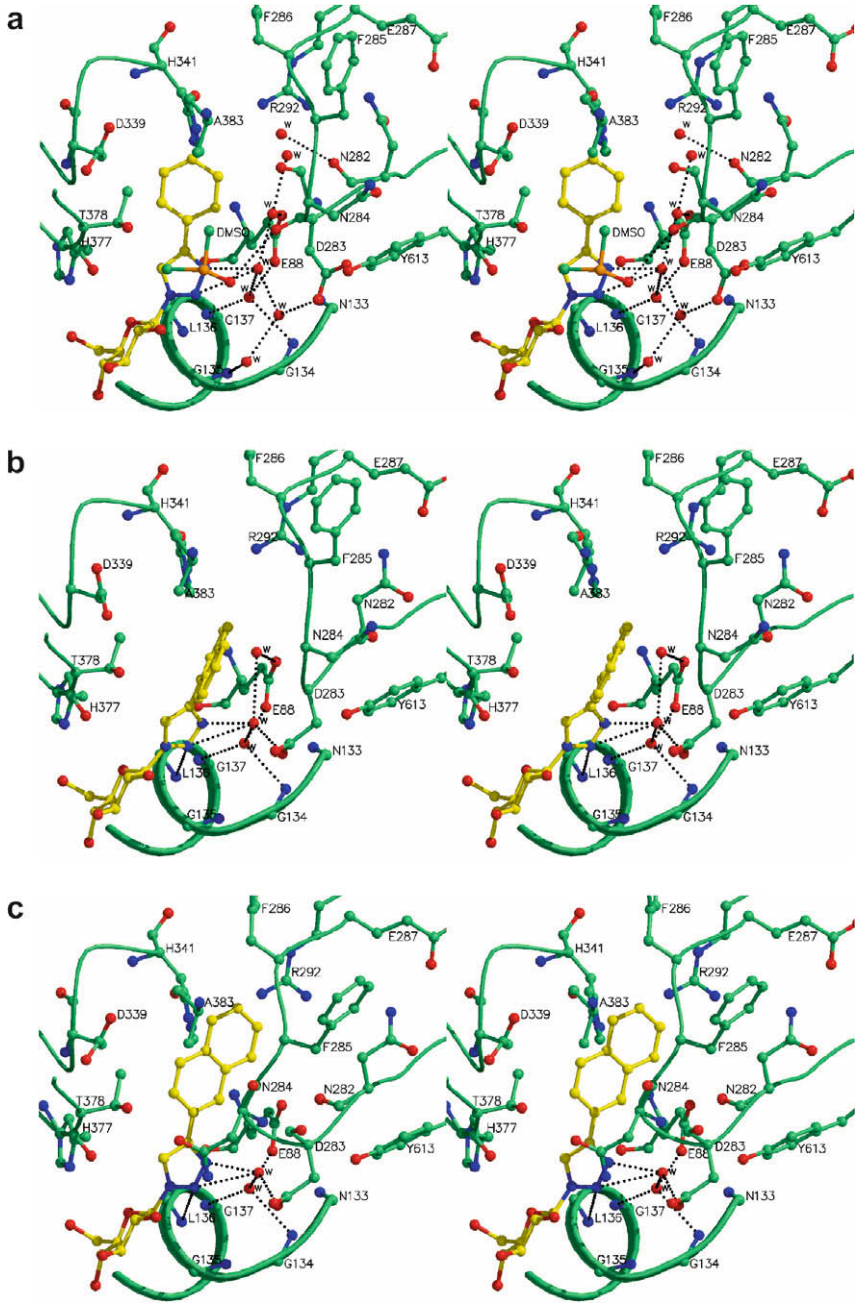

Figure 1. Stereo representation of the molecular interactions of (a) compound **3a** (b) compound **3b**, (c) compound **3d**, (d) compound **5a** and (e) compound **5d** when bound at the catalytic site RMGP*b*. Water molecules are labelled as w. The side chain atoms of residues 136 and 671–676 are not shown for reasons of clarity. The figures were prepared with the program for molecular graphics MOLSCRIPT.[36]

280s loop at the new position, water-mediated hydrogen bond interactions are formed between O2 and Asp283 OD2 through water molecules Wat205 O, Wat70 O and Wat15 O. The latter is a new water molecule occupying the former position of Asp283 side chain that was employed to optimize the network of interactions at the catalytic site. Even if the structural results show that the differences outlined above are significant this is not reflected in the potency of **3a** and **5a** as inhibitors of RMGP*b* indicating that the arrangement of the catalytic site components is almost equally favourable in both complex structures.

2.2. Crystallographic studies: 3b versus 5b

Comparison of RMGP*b*-**3b** and RMGP*b*-**5b** complex structures shows that both compounds are well defined at the catalytic site of the enzyme in accordance with the results obtained from the kinetic studies. In particular, **3b** forms in total 14 hydrogen bonds and 88 van der Waals interactions (Fig. 1b) while **5b** is involved in 13 hydrogen bonds and 99 van der Waals interactions (to be published elsewhere), respectively. The position of glucopyranose is specific and a shift of C1 atom by ~0.6 Å compared to the reference structure RMGP*b*-**5b** is observed. This shift is similar to the one detected in RMGP*b*-**3a** due to the introduction of the triazole moiety. The nitrogen atoms of **3b**, N2 and N3, interact with a direct hydrogen bond with Leu136 N and water-mediated hydrogen bonds with Asp283 OD1 (through Wat64 O), with the glycine-rich helix N atoms of residues Gly134 and Gly137 as well as OE1 and OE2 atoms of Glu88 (through waters Wat63O, Wat64 O and Wat65 O). The naphthyl group adopts a different orientation (rotation by ~160°) with regard to the RMGP*b*-**5b** complex structure as

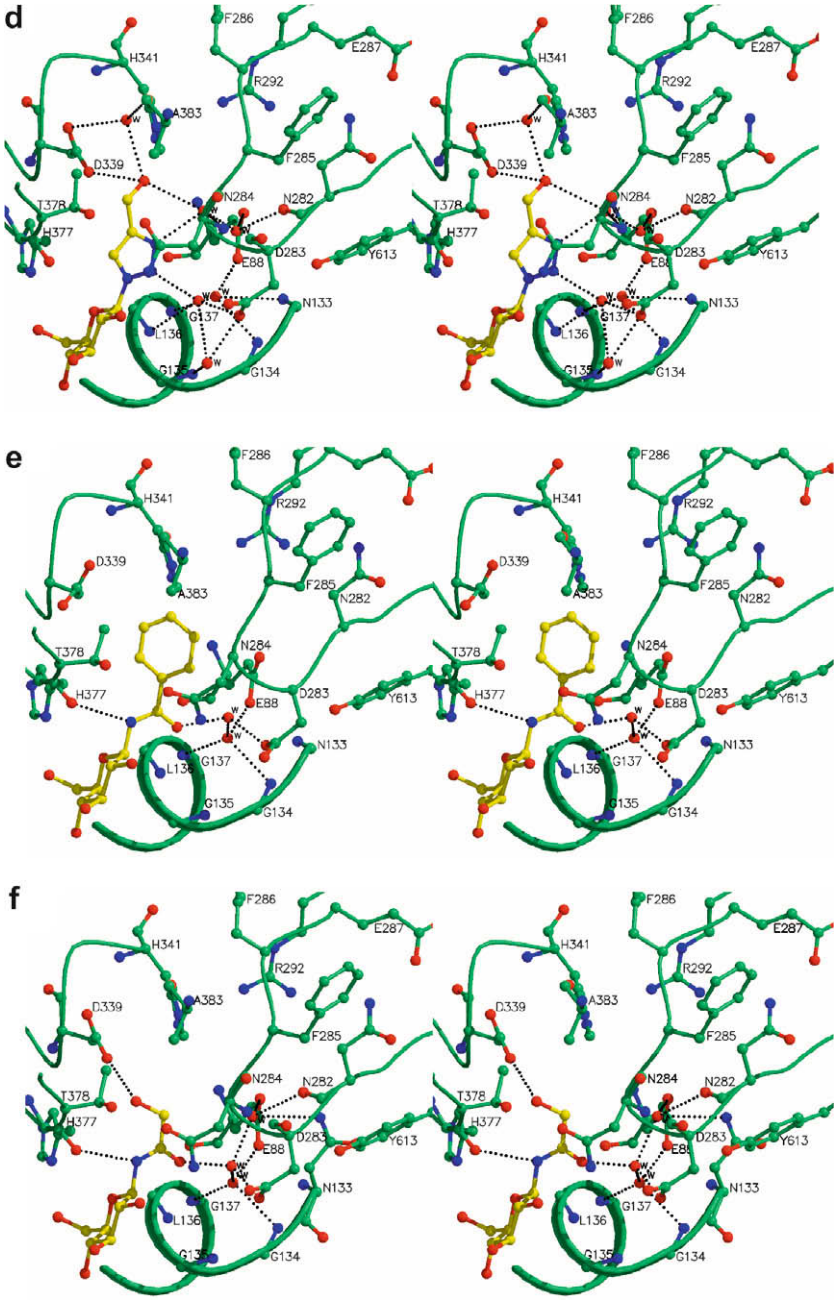

Figure 1. (*continued*)

indicated by both the $2F_o - F_c$ and $F_o - F_c$ electron density maps. The position of the second phenyl group is now occupied by Wat63 O implicated in a network of water-mediated contacts with the triazole nitrogens, described above, optimizing the ligand interactions on binding. The differences observed in the naphthyl group atoms are interrelated with the changes in the 280s loop residues. These involve changes in Asn284 that now points at the inhibitor site between Phe285 and Tyr613 aromatic rings (Cα moves by ~3.5 Å and torsion angles (φ, ψ, $\chi1$, $\chi2$) rotate by (~178, 112, 145, 52) degrees) to avoid clashes with the naphthyl group at its new position. As a result the rest of the residues lining the loop are also subjected to changes in their conformation to satisfy stereochemical conditions imposed by Asn284. These are summarized as follows; Asn282 (Cα atom shifts by ~0.5 Å and torsion angles (ψ, $\chi2$) rotate by (22, 37) degrees), Asp283 (Cα moves by ~0.7 Å and torsion angle ψ rotates by ~113°), Phe285 (Cα shifts by ~2.4 Å and torsion angles (φ, ψ) rotate by (~27, 28) degrees) and Phe286 (Cα shifts by 0.9 Å and torsion angle φ rotates by ~56°). Minor shifts in the range of ~0.4 Å are also recorded for all atoms of His377. Further adjustments in the water structure in the vicinity of the catalytic site are also observed due to the reorganization of the 280s loop residues to improve the overall network of interactions formed on binding of **3b** (e.g., Wat280 located at the inhibitor site in RMGP*b*-**5b** complex is now displaced due to stereochemical clashes with Asn284 side chain atoms and a new water, Wat86 O, is employed to optimize Asn284 interactions at the inhibitor site). Despite the differences mapped upon binding of **3b** to the catalytic site of RMGP*b*, compared to those of **5b**, the number of hydrogen and van der Waals interactions formed between the two inhibitors is equivalent. This finding suggests that

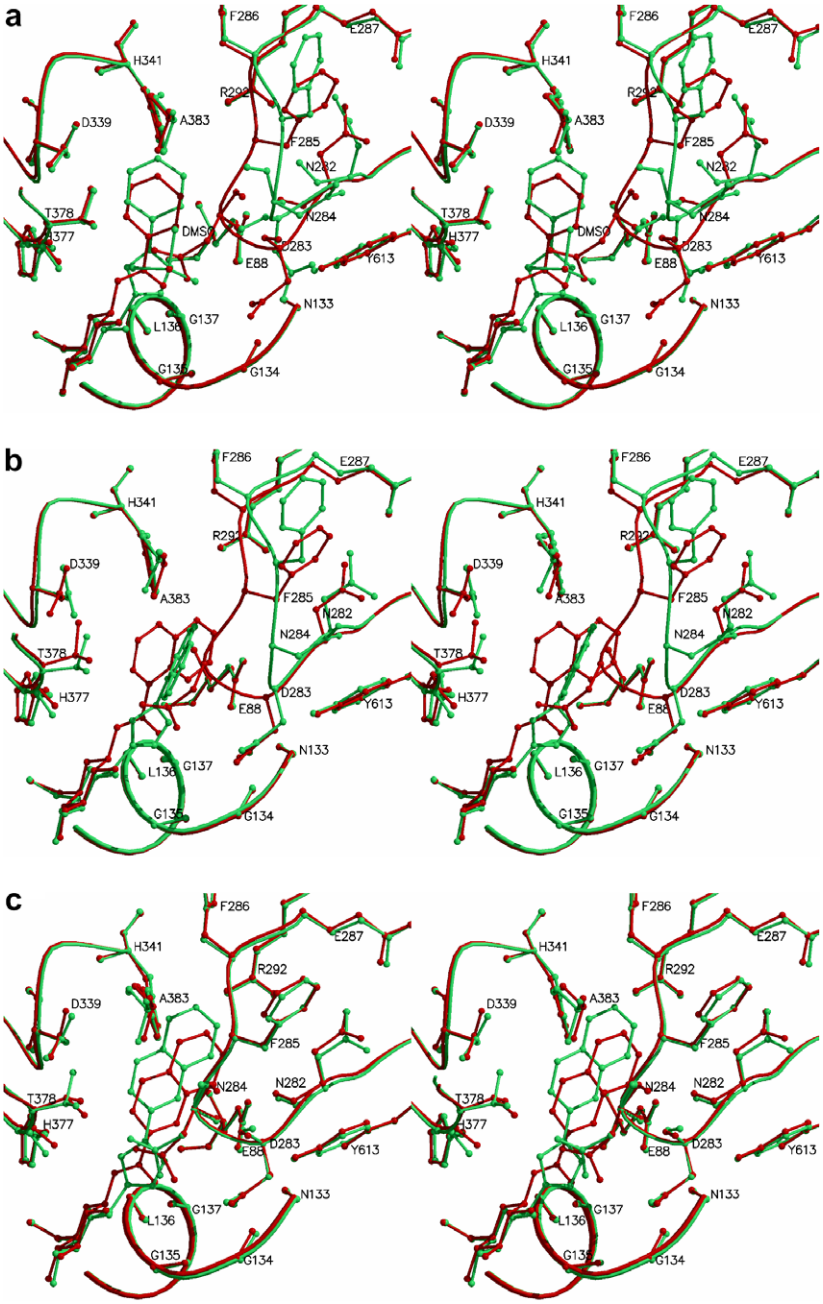

Figure 2. Superpositions of structures obtained for RMGP*b*–inhibitor complexes with amide versus triazole type inhibitors shown in stereo: (a) RMGP*b*-**3a** (in green) and RMGP*b*-**5a** (in red); (b) RMGP*b*-**3b** (in green) and RMGP*b*-**5b** (in red); (c) RMGP*b*-**3c** (in green) and RMGP*b*-**5c** (in red); (d) RMGP*b*-**3d** (in green) and RMGP*b*-**5d** (in red). The figures were prepared with the program for molecular graphics MOLSCRIPT.[36]

the similar inhibition potency exhibited by both compounds might reveal that an energetically favourable conformation is adopted both for 280s loop residues and the ligands in RMGP*b*-**3b** and RMGP*b*-**5b** complex structures.

2.3. Crystallographic studies: 3c versus 5c

It was found that **3c** binds along the catalytic channel of RMGP*b* forming in total 14 hydrogen bonds and 109 van der Waals interactions (Fig. 1c). The naphthyl group occupies the so-called β-pocket, a subsite of the catalytic site, similar to the benzoyl moiety in the RMGP*b*–*N*-benzoyl-*N*′-β-D-glucopyranosylurea (RMGP*b*-Bzurea) complex.[33] In detail, the phenyl group of Bzurea lies next to the 280s catalytic loop as dictated by the orientation of the urea moiety inducing a dramatic shift of the residues lining the loop; this shift is not observed upon binding of **3c** since the atoms forming the urea are now replaced by triazole and the naphthyl ring is accommodated in the β-pocket with no perturbation of the neighbouring residues. The same applies for **5c** in which urea part is also absent and replaced by an amide group. Comparison of **3c** with **5c** binding mode shows no notable changes at the catalytic site of RMGP*b* except small changes in the conformation of Asn284 side chain (ψ rotates by ~27°, atom shifts varying from 0.4 to 0.8 Å), Thr378 (χ1 rotates by 152°) and Wat43 O (Wat109 O in **5c** complex) moves by ~0.8 Å to improve its hydrogen bonding interaction with N3. Overall both **3c** and **5c** bind at RMGP*b* similarly. Although the amide nitrogen N1 of **5c** is hydrogen bonded to His377 O forming a favourable interaction[34,35] characteristic for most glucose

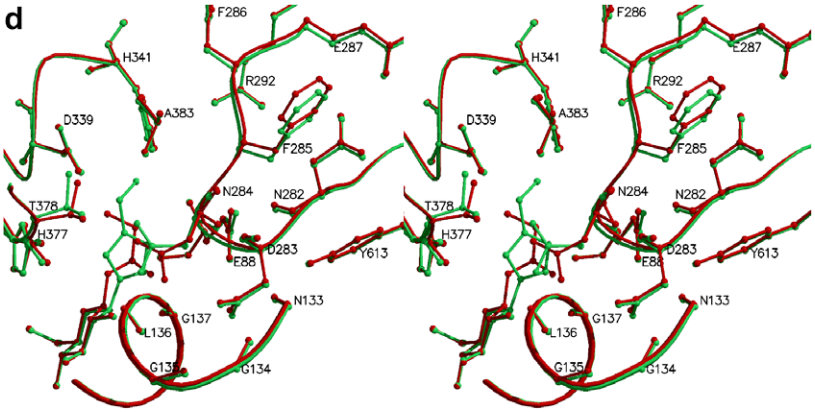

Figure 2. (*continued*)

analogues with an amide group at C1 position of the pyranose ring, it does not exhibit improved affinity for the enzyme compared to **3c**. The absence of the aforementioned interaction in RMGP*b*-**3c** could be counterbalanced by the direct hydrogen bond interaction between N2 and Leu136 N and N3 with Asp283 OD1 (through Wat43 O).

2.4. Crystallographic studies: 3d versus 5d

It was shown that **3d** binds at the catalytic site of RMGP*b* forming a total of 16 hydrogen bonds and 91 van der Waals interactions (Fig. 1d) in a similar fashion to its amide analogue **5d** (14 hydrogen bonds, 89 van der Waals interactions). Although the characteristic hydrogen bond interaction formed between the amide nitrogen of **5d** and the backbone oxygen atom of His377[34,35] is not present in RMGP*b*-**3d** complex structure, it seems that the additional water-mediated interactions formed between N2 and N3 of the ligand with Asp283 OD1, Leu136 N (through Wat245 O) and Asn284 N (through Wat258 O), respectively compensate for this loss resulting in similar affinities. Minor changes are also observed in the catalytic residues Asn284 and Phe285 to optimize the network of interactions upon the binding of **3d**. In detail, $\chi 1$ (N-CA-CB-CG) and $\chi 2$ (CA-CB-CG-OD1) torsion angles rotate by ~51° and ~57°, respectively and all atoms are shifted by an average distance of ~0.6 Å. This change induces shifts in Phe285 atoms by ~0.5 Å. In general, the crystal structures of both **3d** and **5d** do not exhibit overall changes but only localized, favourable though as reflected in their inhibitory effect, alterations in the 280s loop.

3. Conclusion

In conclusion, four pairs of glucose analogue inhibitors of RMGP*b* with amide (NHCO–R) versus 4-R-1,2,3-triazol-1-yl moieties attached to the anomeric carbon exhibited remarkable pairwise coincidence of their inhibitory effect on the enzyme activity. X-ray structural studies of the RMGP*b*-inhibitor complexes revealed binding peculiarities. All ligands bound at the catalytic site of the enzyme at well-defined positions as clearly indicated by the structural data (2.0–2.3 Å resolution for all complexes). In the case of R = Ph, 1-naphthyl derivatives the triazole compounds induced significant conformational changes to the architecture of 280s loop at the catalytic site, mainly caused by flipping of Asn284 side chain that was intercalated between Phe285 and Tyr613 side chains forming the inhibitor site of the enzyme. However, these changes were not observed in the corresponding amide compounds complex structures and the flexibility of the 280s loop residues might explain this difference. In contrast, for R = 2-naphthyl and hydroxymethyl derivatives the binding mode of both triazole and amide compounds proved to be very similar. Although the structural results are directly comparable for only part of the analogues of both series this study provides a new example of the amide-1,2,3-triazole bioisosterism and supports the use of this kind of replacement in medicinal chemistry studies. The architecture of the binding site of interest of the molecular target under investigation should also be taken into consideration in the design of potential bioisosteres.

Acknowledgements

This work was supported by the EU Marie Curie Early Stage Training (EST) Contract No. MEST-CT-020575; a Marie Curie Host Fellowships for the Transfer of Knowledge (ToK) contract no MTKD-CT-2006-042776; the Hellenic General Secretariat for Research and Technology (GSRT), Ministry of Development, through the program 'Excellence in Research Institutes (2nd round)' to N.G.O.; the EMBL-Hamburg outstation under FP6 'Structuring the European Research Area Programme' Contract No. RII3/CT/2004/5060008 and SRS Daresbury Laboratory (contract IHPP HPRI-CT-1999-00012). We are grateful to the staff scientists at EMBL-Hamburg outstation and SRS Daresbury Laboratory for their help during X-ray data collection. Synthetic work in Debrecen was supported by the Hungarian Scientific Research Fund (OTKA 61336 and 68578).

References

1. Patani, G. A.; LaVoie, E. J. *Chem. Rev.* **1996**, *96*, 3147–3176.
2. Lima, L. M. A.; Barreiro, E. J. *Curr. Med. Chem.* **2005**, *12*, 23–49.
3. Wagener, M.; Lommerse, J. P. M. *J. Chem. Inf. Model.* **2006**, *46*, 677–685.
4. Kolb, H. C.; Sharpless, K. B. *Drug Discovery Today* **2003**, *8*, 1128–1137.
5. Moses, J. E.; Moorhouse, A. D. *Chem. Soc. Rev.* **2007**, *36*, 1249–1262.
6. Horne, W. S.; Yadav, M. K.; Stout, C. D.; Ghadiri, M. R. *J. Am. Chem. Soc.* **2004**, *126*, 15366–15367.
7. Appendino, G.; Bacchiega, S.; Minassi, A.; Cascio, M. G.; De Petrocellis, L.; Di Marzo, V. *Angew. Chem., Int. Ed.* **2007**, *46*, 9312–9315.
8. Angell, Y. L.; Burgess, K. *Chem. Soc. Rev.* **2007**, *36*, 1674–1689.
9. Moller, D. E. *Nature* **2001**, *414*, 821–827.
10. Oikonomakos, N. G. *Curr. Protein Pept. Sci.* **2002**, *3*, 561–586.
11. Oikonomakos, N. G.; Somsák, L. *Curr. Opin. Invest. Drugs* **2008**, *9*, 379–395.
12. Somsák, L.; Czifrák, K.; Tóth, M.; Bokor, É.; Chrysina, E. D.; Alexacou, K. M.; Hayes, J. M.; Tiraidis, C.; Lazoura, E.; Leonidas, D. D.; Zographos, S. E.; Oikonomakos, N. G. *Curr. Med. Chem.* **2008**, *15*, 2933–2983.
13. Watson, K. A.; Mitchell, E. P.; Johnson, L. N.; Cruciani, G.; Son, J. C.; Bichard, C. J. F.; Fleet, G. W. J.; Oikonomakos, N. G.; Kontou, M.; Zographos, S. E. *Acta Crystallogr., Sect. D* **1995**, *51*, 458–472.
14. Györgydeák, Z.; Hadady, Z.; Felföldi, N.; Krakomperger, A.; Nagy, V.; Tóth, M.; Brunyánszky, A.; Docsa, T.; Gergely, P.; Somsák, L. *Bioorg. Med. Chem.* **2004**, *12*, 4861–4870.
15. Kovács, L.; Ősz, E.; Domokos, V.; Holzer, W.; Györgydeák, Z. *Tetrahedron* **2001**, *57*, 4609–4621.
16. Somsák, L.; Kovács, L.; Tóth, M.; Ősz, E.; Szilágyi, L.; Györgydeák, Z.; Dinya, Z.; Docsa, T.; Tóth, B.; Gergely, P. *J. Med. Chem.* **2001**, *44*, 2843–2848.

17. *Compound* **3a**. 1-(β-D-Glucopyranosyl)-4-phenyl-1,2,3-triazole: white solid. Mp: 228–231 °C (lit.[25] mp: 228–230 °C); $[\alpha]_D = -69$ (*c* 0.24, DMSO).
18. *Compound* **3b**. 1-(β-D-Glucopyranosyl)-4-(1-naphthyl)-1,2,3-triazole: colourless syrup. R_f: 0.35 (8:2 $CHCl_3$–MeOH); $[\alpha]_D = -22$ (*c* 0.21, MeOH); ^{1}H NMR (CD_3OD) δ (ppm) 8.48 (1H, s, triazole H), 8.20–7.44 (7H, m, aromatics), 5.75 (1H, d, $J_{1',2'}$ 9.2 Hz, H-1′), 4.05 (1H, pseudo t, $J_{2',3'}$ 9.2, H-2′), 3.91 (1H, dd, $J_{5',6'a}$ <1 Hz, $J_{6'a,6b}$ 11.9 Hz, H-6′a), 3.73 (1H, dd, $J_{5',6'b}$ 5.3 Hz, H-6′b), 3.68–3.55 (3H, m, H-3′, H-4′, H-5′); ^{13}C NMR (CD_3OD) δ (ppm) 147.5 (triazole C-4), 135.3, 132.3, 130.3, 129.5, 128.5, 127.2, 127.8, 126.4, 126.2, (aromatics), 124.5 (triazole C-5), 89.8 (C-1′), 81.1, 78.4, 74.0, 70.8 (C-2′–C-5′), 62.3 (C-6′). Anal. Calcd for $C_{18}H_{19}N_3O_5$ (357.37): C, 60.50; H, 5.36; N, 11.76. Found: C, 60.42; H, 5.25; N, 11.69.
19. *Compound* **3c**. 1-(β-D-Glucopyranosyl)-4-(2-naphthyl)-1,2,3-triazole: white solid. Mp: 212–214 °C; $[\alpha]_D = -26$ (*c* 0.21, DMSO); ^{1}H NMR (DMSO-d_6) δ (ppm) 8.98 (1H, s, triazole H), 8.47 (1H, s, aromatic), 8.01–7.92 (4H, m, aromatics), 7.53 (2H, m, aromatics), 5.62 (1H, d, $J_{1',2'}$ 7.9 Hz, H-1′), 5.50 (1H, d, *J* 4.0 Hz, OH), 5.38 (1H, d, *J* 2.6 Hz, OH), 5.22 (1H, d, *J* 4.0 Hz, OH), 4.68 (1H, t, OH), 3.84–3.29 (6H, m, H-2′, H-3′, H-4′, H-5′, H-6′ab); ^{13}C NMR (DMSO-d_6) δ (ppm) 146.3 (triazole C-4), 133.1, 132.5, 128.5, 128.0, 127.9, 127.7, 126.6, 126.1, 123.6, 123.4, (aromatics), 120.8 (triazole C-5), 87.7 (C-1′), 79.9, 76.8, 72.2, 69.6 (C-2′–C-5′), 60.7 (C-6′). Anal. Calcd for $C_{18}H_{19}N_3O_5$ (357.37): C, 60.50; H, 5.36; N, 11.76. Found: C, 60.61; H, 5.31; N, 11.82.
20. *Compound* **3d**. 1-(β-D-Glucopyranosyl)-4-hydroxymethyl-1,2,3-triazole: white solid. Mp: 156–158 °C (lit.[26] mp: 162–163 °C); $[\alpha]_D = -5$ (*c* 0.16, H_2O).
21. *Compound* **4d**. *N*-Acetoxyacetyl-2,3,4,6-tetra-*O*-acetyl-β-D-glucopyranosylamine: colourless syrup. R_f: 0.24 (1:1 EtOAc–hexane), $[\alpha]_D = +59$ (*c* 0.24, $CHCl_3$); ^{1}H NMR ($CDCl_3$) δ (ppm) 7.05 (1H, d, $J_{1,NH}$ 9.2 Hz, NH), 5.33, 5.24, 5.08, 4.96 (4 × 1H, 4 pseudo t, *J* 9.2, 10.6 Hz in each, H-1, H-2, H-3, H-4), 4.69, 4.43 (2 × 1H, 2d, *J* 15.9 Hz,CH_2a, CH_2b), 4.33 (1H, dd, $J_{6a,6b}$ 13.2 Hz, H-6a), 4.09 (1H, dd, $J_{5,6b}$ 2.6 Hz, H-6b), 3.86 (1H, ddd, $J_{5,6a}$ 5.3 Hz, H-5), 2.20, 2.09, 2.05, 2.04, 2.03 (15H, 5s, 5 × CH_3); ^{13}C NMR ($CDCl_3$) δ (ppm) 171.3, 170.5, 169.7, 169.6, 169.4, 167.9 (CO), 77.8 (C-1), 73.6, 72.3, 70.2, 68.0 (C-2–C-5), 62.4, 61.4 (C-6, CH_2), 20.6, 20.4 (4) (CH_3). Anal. Calcd for $C_{18}H_{25}NO_{12}$ (447.40): C, 48.32; H, 5.63; N, 3.13. Found: C, 48.41; H, 5.22; N, 3.02.
22. *Compound* **5d**. *N*-Hydroxyacetyl-β-D-glucopyranosylamine: white crystals. Mp: 150–152 °C; $[\alpha]_D = -2$ (*c* 0.22, MeOH); ^{1}H NMR (CD_3OD) δ (ppm) 4.95 (1H, d, $J_{1,2}$ 9.2 Hz, H-1), 4.05 (2H, s, CH_2), 3.83 (1H, dd, $J_{5,6a}$ <1 Hz, $J_{6a,6b}$ 11.9 Hz, H-6a), 3.67 (1H, dd, $J_{5,6b}$ 5.3 Hz, H-6b), 3.46–3.31 (4H, m, H-2, H-3, H-4, H-5); ^{13}C NMR (CD_3OD) δ (ppm) 176.3 (CO), 80.7 (C-1), 79.7, 78.8, 73.8, 71.3 (C-2–C-5), 62.7, 62.6 (C-6, CH_2). Anal. Calcd for $C_8H_{15}NO_7$ (237.21): C, 40.51; H, 6.37; N, 5.90. Found: C, 40.03; H, 6.30; N, 5.99.

23. Akula, R. A.; Temelkoff, D. P.; Artis, N. D.; Norris, P. *Heterocycles* **2004**, *63*, 2719–2725.
24. Chittaboina, S.; Xie, F.; Wang, Q. *Tetrahedron Lett.* **2005**, *46*, 2331–2336.
25. Rossi, L. L.; Basu, A. *Bioorg. Med. Chem. Lett.* **2005**, *15*, 3596–3599.
26. Wilkinson, B. L.; Bornaghi, L. F.; Poulsen, S.-A.; Houston, T. A. *Tetrahedron* **2006**, *62*, 8115–8125.
27. Oikonomakos, N. G.; Kontou, M.; Zographos, S. E.; Watson, K. A.; Johnson, L. N.; Bichard, C. J. F.; Fleet, G. W. J.; Acharya, K. R. *Protein Sci.* **1995**, *4*, 2469–2477.
28. Saheki, S.; Takeda, A.; Shimazu, T. *Anal. Biochem.* **1985**, *148*, 277–281.
29. Oikonomakos, N. G.; Melpidou, A. E.; Johnson, L. N. *Biochim. Biophys. Acta* **1985**, *832*, 248–256.
30. Otwinowski, Z.; Minor, W. *Methods Enzymol.* **1997**, *276*, 307–326.
31. CCP4. *Acta Crystallogr. Sect. D* **1994**, *50*, 760–763.
32. Watson, K. A.; Chrysina, E. D.; Tsitsanou, K. E.; Zographos, S. E.; Archontis, G.; Fleet, G. W. J.; Oikonomakos, N. G. *Proteins: Struct. Funct. Bioinform.* **2005**, *61*, 966–983.
33. Oikonomakos, N. G.; Kosmopolou, M.; Zographos, S. E.; Leonidas, D. D.; Somsák, L.; Nagy, V.; Praly, J.-P.; Docsa, T.; Tóth, B.; Gergely, P. *Eur. J. Biochem.* **2002**, *269*, 1684–1696.
34. Bichard, C. J. F.; Mitchell, E. P.; Wormald, M. R.; Watson, K. A.; Johnson, L. N.; Zographos, S. E.; Koutra, D. D.; Oikonomakos, N. G.; Fleet, G. W. J. *Tetrahedron Lett.* **1995**, *36*, 2145–2148.
35. Gregoriou, M.; Noble, M. E. M.; Watson, K. A.; Garman, E. F.; Krülle, T. M.; Fuente, C.; Fleet, G. W. J.; Oikonomakos, N. G.; Johnson, L. N. *Protein Sci.* **1998**, *7*, 915–927.
36. Kraulis, P. *J. Appl. Crystallogr.* **1991**, *24*, 946–950.